

Cirrus Cloud Radiative Forcing Derived from Synergetic Use of MODIS Analyses and Ground-Based Observations

Shuichiro Katagiri¹, Nobuyuki Kikuchi², Takashi Y. Nakajima³, Akiko Higurashi², Atsushi Shimizu², Ichiro Matsui², Tadahiro Hayasaka⁴, Nobuo Sugimoto², Tamio Takamura⁵, and Teruyuki Nakajima⁶

¹Japan Aerospace Exploration Agency, Tsukuba, Japan

²National Institute for Environmental Studies, Tsukuba, Japan

³Tokai University, Tokyo, Japan

⁴Tohoku University, Tokyo, Japan

⁵Chiba University, Chiba, Japan

⁶The University of Tokyo, Kashiwa, Japan

Abstract

We have been performing radiative budget measurements at a ground-based observatory located on Fukue Island. In this study, we analyzed the data from instruments installed in the observatory and the data observed by MODIS, the satellite-borne imager, to evaluate cirrus cloud radiative forcing (CRF). The result shows that CRF took a large positive value as 127.98 W m^{-2} at the top of the atmosphere (TOA) and a small positive value as 13.2 W m^{-2} at the surface. As a result, it was found that optically very thin cirrus clouds exert a strong warming effect on the Earth's system and a weak warming effect on the Earth's surface when aerosols are not taken into account.

1. Introduction

Cirrus clouds play an important role in the radiative forcing on the Earth's climate (Liou 1986; Schlimme et al. 2005). Cirrus clouds affect climate in two opposite ways such as reflecting sunlight, i.e., the albedo effect, and absorbing terrestrial radiation, i.e. the greenhouse effect. The balance between these two processes determines the net impact of cirrus clouds. Therefore, CRF is a very important parameter to quantify the impact of cirrus clouds (Chen et al. 2000; Chylek and Wong 1998). The net CRF at TOA in the Indian Ocean region was studied using ERBE satellite data and was found to be strongly affected by the high cloud amount, but to weakly depend on the changes in low or middle clouds (Pai and Rajeevan 1998). Therefore, to understand the climate system the role of cirrus clouds has to be comprehended, though this task is not easy to manage because we need observation from both the ground and aircrafts or satellites to fully depict radiative budget change in all altitudes.

In this paper, we reconstructed a radiative field observed at the Fukue Observatory and evaluated the CRF caused by cirrus clouds.

2. Data source and radiative transfer model

We have observed several radiative properties at the observatory located on Fukue Island as illustrated in Fig. 1 (referred to as the Fukue site hereafter). In this study, we used ground-based data obtained from a Kip & Zonen CM21 pyranometer, a Kip & Zonen CG4 pyrgeometer, and a RPG microwave radiometer. The lidar data was provided by the NIES (the National Institute for Environmental Studies). This lidar system was developed by the NIES with wavelengths of 532 nm and 1,064 nm and with a depolariza-

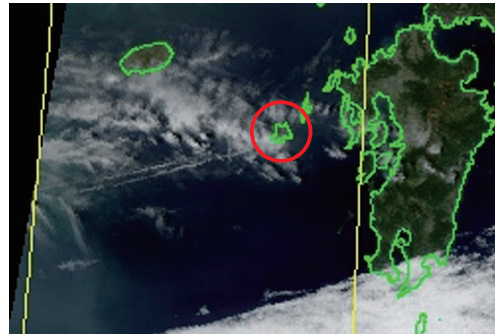


Fig. 1. A visible composite scene from MODIS data over the Fukue site as encircled. The cirrus edge covers the site.

tion measurement capability at 532 nm. The all-sky photographs were taken by a PREDE Sky View camera.

Besides the ground-based data, we used data, derived from satellite observation by the Moderate Resolution Imaging Spectroradiometer (MODIS), such as cloud optical thickness (COT), cloud effective radius (RE), aerosol optical thickness (AOT), and Ångström parameter (ANG). COT and RE were derived from a solar reflective method for water clouds, named the Comprehensive Analysis Program for Cloud Optical Measurements (CAPCOM) (Nakajima and Nakajima 1995; Kawamoto et al. 2001). The aerosol parameters, AOT and ANG, were retrieved with the two-channel aerosol retrieval algorithm (Higurashi and Nakajima 1999; Higurashi et al. 2000).

We used the FSTAR code of OpenCLASTR for radiative flux calculation (Nakajima and Tanaka 1986, 1988) with the LOWTRN-7 gas absorption model (Kneizys et al. 1988). The look-up tables were used for MODIS data retrievals of the cloud parameters and the aerosol parameters were also constructed using OpenCLASTR RSTAR code.

3. Observed parameters at the Fukue observatory

Figure 1 shows a visible composite of MODIS data obtained at around 10:30 a.m. JST on April 16, 2004, in which the Fukue site (encircled) is almost covered by the optically thin cloud. Therefore, we were able to derive both the cloud and aerosol microphysical parameters near the Fukue site from MODIS data analysis and simultaneously compare the ground-based observation data. The photograph of the entire sky above the Fukue site is shown in Fig. 2, which also consistently indicates existence of the cirrus above the Fukue site. The horizontal distribution of AOT and ANG derived from MODIS data are shown in Fig. 3, from which we obtained AOT and ANG values as 0.55 and 0.7

above the Fukue site, respectively. Figure 3 also shows the optically equivalent aerosol types from MODIS data, in which four colors—red, yellow, green, and blue—express soil dust, carbonaceous, sulfate, and sea salt aerosols, respectively. Sulfate aerosol is seen around the Fukue site in the figure.

We obtained the sum value of the optical thickness of clouds and aerosols (CAOT) and RE at the Fukue site as 3.88 and 26 μm , respectively, though they are not shown in the figures. Here, we have to note that the algorithm used for this cloud analysis was the algorithm for water clouds (CAPCOM). Figure 4 shows NIES lidar data of lidar intensity at 532 nm, depolarization ratio at 532 nm, and intensity ratio between 1064 nm and 532 nm, from which we recognized the top and bottom height of cirrus are 10 km and 8 km, respectively. The figure also shows existence of an aerosol layer below the height of 3 km over the Fukue site. Large depolarization ratio suggests this aerosol layer is composed of non-spherical dust aerosol. The dust aerosol layer is covered and mixed by a small and spherical aerosol layer, but we were not able to discriminate the species of this spherical aerosol. Analysis of the lidar data with forward calculation is shown in Fig. 5 (Shimizu A. et al. 2004; Nishizawa et al. 2007). Observed radiative fluxes at the Fukue site are shown in Table 1, i.e., the shortwave flux from the pyranometer was 832.7 W m^{-2} and the longwave flux from the pyrgeometer was 297.1 W m^{-2} . We also summarized obtained parameters of the cloud and aerosol in Table 1. There are several inconsistencies between the data from the satellite and the ground-based measurements. AOT value of 0.55 observed by MODIS is larger than 0.23, the total amount of AOT for dust and spherical types observed by the lidar. Figure 4 suggests that optically thin cirrus contaminated satellite retrievals in the region close to Fukue site. ANG was also contaminated by cirrus and therefore estimated to be a smaller value.

On the other hand, the MODIS AOT value of about 0.35 in the region off Fukue Island toward North is considered to be a cirrus free value and is more consistent with the lidar value. CAOT value from MODIS is the sum of COT of the cirrus and AOT of both dust and spherical aerosols so that the value of 3.88 should be regarded as the total optical thickness at the Fukue site.

If we subtract AOT = 0.23 from the lidar, we have a cirrus optical thickness of 3.65. The liquid water path (LWP) can be retrieved by a microwave radiometer as 50 g m^{-2} at the Fukue site. It is, however, difficult to estimate the ice water path (IWP) in the case of cirrus because the scattering efficiency factor depends on the shape and orientation of ice particles, and usually it is larger than that of a water cloud.

In this study, we assume the ice particle of the cirrus as spherical and as having the same scattering efficiency factor as that of the water particle. The pseudo water particle size, RE_{pseudo} can be calculated by

$$RE_{\text{pseudo}} \approx \frac{3 LWP}{2 COT}, \quad (1)$$

then we obtained $RE_{\text{pseudo}} = 20.5 \mu\text{m}$. The actual size of the ice particle, RE_{ice} , is larger than RE_{pseudo} and smaller than RE (= 26 μm) because the larger scattering efficiency factor of ice particles reduces the value of LWP, from the microwave radiometer. The smaller reflectivity also increases the value of RE derived from MODIS with the reflection method, e.g., a 10 percent reduction of reflectance in near infrared causes an RE increase of about 50 percent for each 20 μm particle. Therefore, we assumed RE_{ice} as 24 μm for flux calculations. This assumption will not cause a large error because differences among satellite and ground-based estimates are within 20 percent of 24 μm .



Fig. 2. An all-sky view from the Fukue site shot at almost the same time as when MODIS crossed over. The Fukue site was covered by the edge of the cirrus at 10:30 a.m. JST on April 16, 2004.

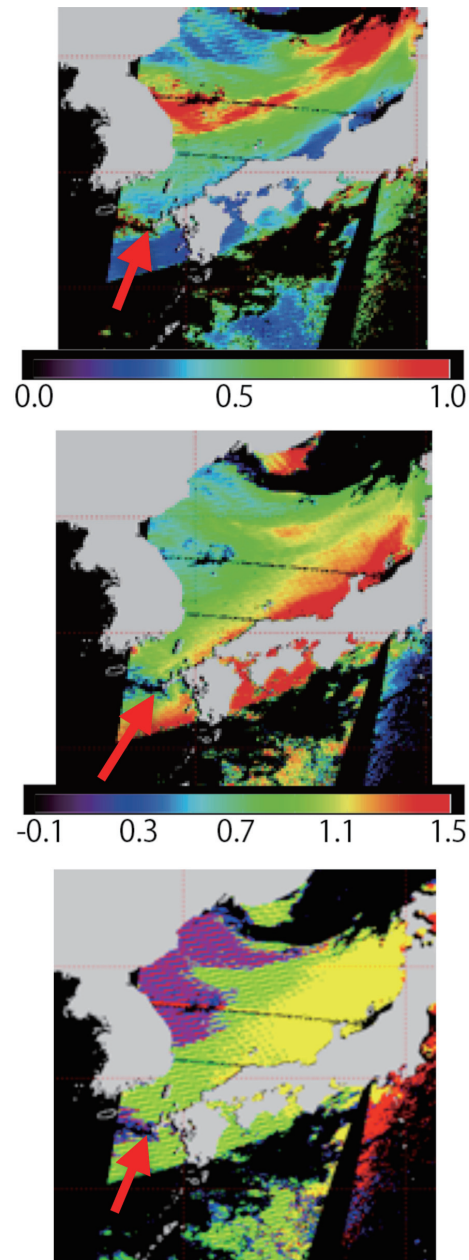


Fig. 3. Aerosol parameters derived from MODIS: AOT (top), ANG (middle), and aerosol type (bottom). Aerosol types of soil dust, carbonaceous, sulfate, and sea salt are indicated in red, yellow, green, and blue, respectively. The red arrow points at the Fukue site.

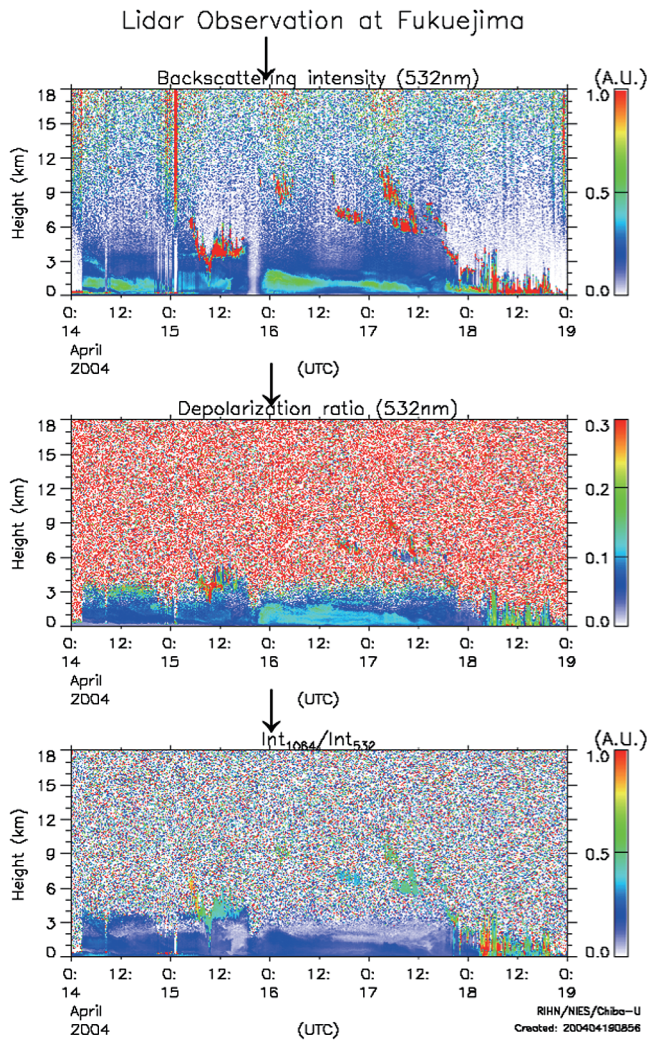


Fig. 4. Lidar observation at Fukue site. Backscattering lidar intensity at 532 nm, depolarization ratio at 532 nm, and intensity ratio between 1064 nm and 532 nm are shown in top, middle, and bottom panels, respectively. Arrows indicate the crossing time of MODIS over the Fukue site.

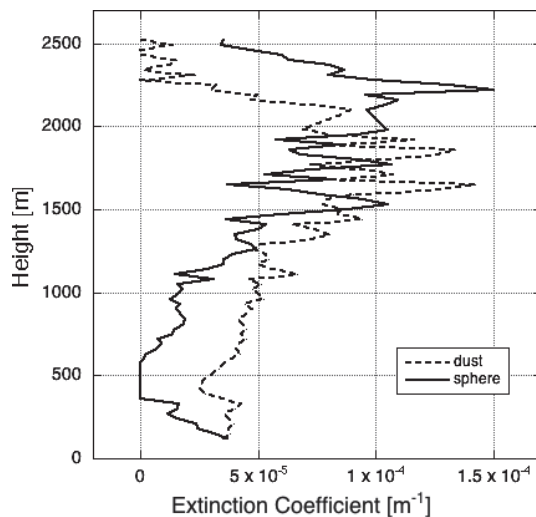


Fig. 5. Extinction coefficient profiles derived from the Lidar data. Dashes and solid lines indicate the extinction coefficient of dust and spherical aerosols, respectively.

4. Flux calculations

We tried to reproduce the fluxes, 832.7 W m^{-2} and 297.1 W m^{-2} , obtained by the pyranometer and the pyrgeometer on the ground, respectively, with the other observed data as listed in Table 1 using the FSTAR code. In the first calculation, we assumed $COT_{\text{cirrus}} = 3.65$ and $RE_{\text{cirrus}} = 24 \mu\text{m}$, and calculated a total cloudy case. We also assumed a two-component aerosol mixture of non-spherical Asian sand particles (yellow sand model of FSTAR) with $AOT = 0.126$ and spherical sulfate aerosol with $AOT = 0.107$.

Then, we obtained a smaller shortwave flux (787.0 W m^{-2}) and a larger longwave flux (308.0 W m^{-2}). This type of discrepancy can be caused by overestimation of COT_{cirrus} . Hence, we reduced COT_{cirrus} from 3.65 to 2.01, which resulted in shortwave and longwave fluxes of 832.6 and 300.4, respectively, which are very close to the observed values on the ground.

The calculation described above indicates that there exists an inconsistency between MODIS-derived COT and radiative fluxes observed on the ground. We are not able to identify the cause of this error, but there must be several causes, such as cloud inhomogeneity in the horizontal distribution of COT and errors caused by the shape and/or the orientation of ice crystals. The radiative properties of cirrus depend on the shapes and sizes of ice crystals, such that the cirrus cloud albedo varies largely according to its shape when the total volume is the same.

Table 1. Summary of Data for Flux Calculations.

Parameters	Values	unit
RE from MODIS	26	μm
RE from Microwave Radiometer	20.5	μm
COT from MODIS	3.88 (3.65)(2.01)	
AOT from MODIS	0.55 (0.35)	
AOT (dust) form Lidar	0.1263	
AOT (sphere) form Lidar	0.1068	
ANG from MODIS	0.7 (larger)	
Pyranometer	832.7	W m^{-2}
Pyrgeometer	297.1	W m^{-2}
LWP from Microwave Radiometer	50	g m^{-2}
IWV from Microwave Radiometer	8.8	kg m^{-2}
Cloud Top Temperature form MODIS	220	K
Cloud Top Height from Lidar	10	km
Cloud Bottom Height from Lidar	8	km
Surface Temperature	293.5	K
Aerosol Species from MODIS	Sulfate	

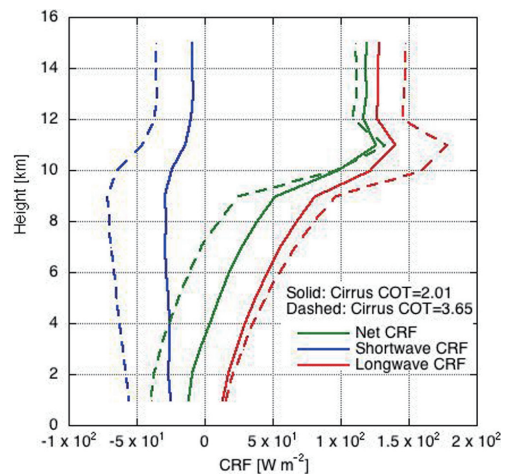


Fig. 6. Calculated Cirrus Cloud Radiative Forcing including the aerosol in the lower atmosphere. Green, red, and blue lines show net CRF, longwave CRF, and shortwave CRF, respectively. The solid lines show cases of $COT = 2.01$, and the dashed lines show cases of $COT = 3.65$.

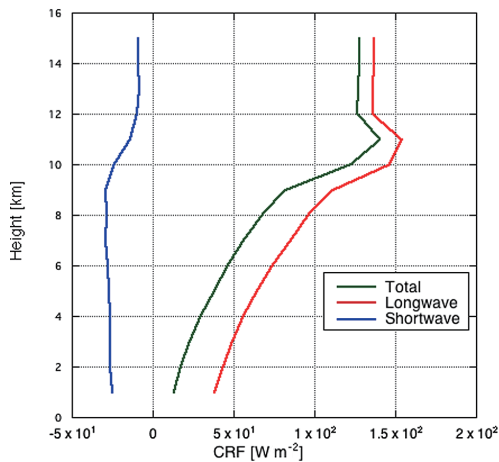


Fig. 7. Same as Fig. 6 but in the case of $COT = 2.01$ and without aerosol in lower part of the atmosphere.

Figure 6 shows calculated cirrus CRF profiles assuming $COT = 2.01$ at the time of MODIS crossing over the Fukue site, where the green, red, and blue lines show the total CRF, the shortwave CRF, and the longwave CRF, respectively. Figure 7 shows the same as Fig. 6, but without aerosol in the lower part of the atmosphere. We can see that the cirrus exerts a strong warming effect on the Earth's system and a weak warming effect on the ground. In this case, aerosols exert a weak cooling effect. Mace et al. (2006) also found that thin high clouds (base > 6.5 km, $\tau < 5$) resulted in warming 25 W m^{-2} at TOA during 2000.

In Fig. 7, the shortwave CRF indicates a weak reflection of 9.0 W m^{-2} by cirrus clouds, while the longwave CRF indicates strong absorption of 155.1 W m^{-2} . The largest net CRF is about 140 W m^{-2} at an altitude of 11 km, heating the upper atmosphere significantly. Its effect extends down to the ground surface level. We have the net CRF of 127.98 W m^{-2} and 13.2 W m^{-2} at TOA and at the surface, respectively. In another calculation of the CRF in Fig. 6 with the aerosol layer in the lower atmosphere, we had the net CRF of 118.98 W m^{-2} at TOA and -12.0 W m^{-2} on the surface, respectively.

5. Conclusion

The calculated cirrus CRF indicates that optically thin cirrus can impact the Earth's climate warming the atmosphere, especially at high altitudes. This large positive forcing will be significantly reduced when the satellite value of $COT = 3.65$ is adopted. This fact clearly suggests that a synergetic use of satellite and surface measurements of pyranometer, pyrgeometer, and lidar is very important when confirming that the satellite COT and RE are consistent with the surface-observed radiative flux, hence the validity of CRF derived from satellite-only measurement. It is, therefore, very important to advance collocation of the surface radiative flux network, such as the BSRN, lidar network, and SKYNET, which uses these two instruments (Nakajima et al. 2007).

Acknowledgments

This study was supported by the projects of JAXA/ Earth-CARE, MEXT/VL for Climate System Diagnostics, MOE/Global Environment Research Fund B-083, and NIES/GOSAT.

References

- Chen, T., W. B. Rossow, and Y. C. Zhang, 2000: Radiative effects of cloud-type variations, *J. Climate*, **13**, 264–286.
- Chylek, P., and J. G. D. Wong, 1998: Cloud radiative forcing ratio – An analytical model, *Tellus A*, **50**, 259–264.
- Higurashi, A., and T. Nakajima, 1999: Development of a two-channel aerosol retrieval algorithm on global scale using NOAA/AVHRR, *J. Atmos. Sci.*, **56**, 924–941.
- Higurashi, A., T. Nakajima, B. N. Holben, A. Smirnov, R. Frouin, and B. Chatenet, 2000: A global characterization of aerosols with two-channel remote sensing, *J. Climate*, **13**, 2011–2027.
- Kawamoto, K., T. Nakajima, and T. Y. Nakajima, 2001: A global determination of cloud microphysics with AVHRR remote sensing, *J. Climate*, **14**, 2054–2068.
- Liou, K.-N., 1986: The influence of cirrus on weather and climate processes: A global perspective, *Mon Wea. Rev.*, **114**, 1167–1199.
- Mace, G. G., S. Benson, and S. Kato, 2006: Cloud radiative forcing at the Atmospheric Radiation Measurement Program Climate Research Facility: 2. Vertical redistribution of radiant energy by clouds, *J. Geophys. Res.*, **111**, D11S91, doi:10.1029/2005JD005922.
- Nakajima, T., and M. Tanaka, 1986: Matrix formulation for the transfer of solar radiation in a plane-parallel scattering atmosphere, *J. Quant. Spectrosc. Radiat. Transfer*, **35**, 13–21.
- Nakajima, T., and M. Tanaka, 1988: Algorithms for radiative intensity calculations in moderately thick atmospheres using a truncation approximation, *J. Quant. Spectrosc. Radiat. Transfer*, **40**, 51–69.
- Nakajima, T., and A. Higurashi, 1998: A use of two-channel radiances for an aerosol characterization from space, *Geophys. Res. Lett.*, **25**, 3815–3818.
- Nakajima, T. Y., and T. Nakajima, 1995: Wide-area determination of cloud microphysical properties from NOAA AVHRR measurements for FIRE and ASTEX regions, *J. Atmos. Sci.*, **52**, 4043–4059.
- Nakajima, T., S. C. Yoon, V. Ramanathan, G. Y. Shi, T. Takemura, A. Higurashi, T. Takamura, K. Aoki, B. J. Sohn, S. W. Kim, H. Tsuruta, N. Sugimoto, A. Shimizu, H. Tanimoto, Y. Sawa, N.-H. Lin, C. T. Lee, D. Goto, and N. Schutgens, 2007: Overview of the Atmospheric Brown Cloud East Asian Regional Experiment 2005 and a study of the aerosol direct radiative forcing in East Asia, *J. Geophys. Res.*, **112**, D24S91, doi:10.1029/2007JD009009.
- Nishizawa, T., H. Okamoto, N. Sugimoto, I. Matsui, A. Shimizu, and K. Aoki, 2007: An algorithm that retrieves aerosol properties from dual-wavelength polarized lidar measurements, *J. Geophys. Res.*, **112**, D06212, doi:10.1026/2006JD007435.
- Pai, D. S., and M. Rajeevan, 1998: Clouds and cloud radiative forcing over tropical Indian Ocean and their relationship with sea surface temperature, *Curr. Sci.*, **75**, 372–381.
- Schlimme, I., A. Macke, and J. Reichardt, 2005: The impact of ice crystal shapes, size distributions, and spatial structure of cirrus clouds on solar radiative fluxes, *J. Atmos. Sci.*, **62**, 2274–2283.
- Shimizu, A., N. Sugimoto, I. Matsui, K. Arai, I. Uno, T. Murayama, N. Kagawa, K. Aoki, A. Uchiyama, and A. Yamazaki, 2004: Continuous observations of Asian dust and other aerosols by polarization lidar in China and Japan during ACE-Asia, *J. Geophys. Res.*, **109**, D19S17, doi:10.1029/2002JD003253.
- Stamnes, K., S. C. Tsay, W. Wiscombe, and K. Jayaweera, 1988: Numerically stable algorithm for discrete-ordinate-method radiative transfer in multiple scattering and emitting layered media, *Appl. Opt.*, **27**, 2502–2509.